Title
Scaling trends of the critical E × B shear for edge harmonic oscillation onset in DIII-D quiescent H-mode plasmas

Journal
Nuclear Fusion, 58(11)

ISSN
0029-5515

Authors
Wilks, TM
Garofalo, AM
Diamond, PH
et al.

Publication Date
2018-11-01

DOI
10.1088/1741-4326/aad143

Peer reviewed

Scaling trends of the critical ExB shear for edge harmonic oscillation onset in DIII-D quiescent H-mode plasmas

To cite this article before publication: Theresa M Wilks *et al* 2018 *Nucl. Fusion* in press https://doi.org/10.1088/1741-4326/aad143

Scaling Trends of the Critical ExB Shear for Edge Harmonic Oscillation Onset in DIII-D Quiescent H-mode Plasmas

T.M. Wilks[1], A.M. Garofalo[2], P.H. Diamond[3], Z.B. Guo[3], J.W. Hughes[1], K.H. Burrell[2], and Xi Chen[2]

[1]MIT-PSFC, [2]General Atomics, [3]UCSD

Abstract

Quiescent H-mode (QH-mode) has been identified as an attractive stationary operational regime in tokamaks due to its lack of edge localized modes (ELMs), along with good particle and impurity control aided by the presence of magnetohydrodynamic modes such as the edge harmonic oscillation (EHO) or edge turbulence. Experiments on the DIII-D tokamak explore local access conditions for QH-mode through measurements of the critical edge rotational shear necessary for the transition from a QH-mode with a coherent EHO to a typical ELMy H-mode. The critical ExB shear and EHO frequency are predicted by a nonlinear phase-dynamics model relating the pressure and velocity perturbations in the edge pedestal region. The reduced theoretical model predicts a linear relationship between critical shearing rate and $c_s/\sqrt{L_p \Delta x}$, where c_s is the ion acoustic velocity, L_p the pressure gradient scale length, and Δx the radial width of the mode. This scaling of the critical shearing rate agrees with the experimental trend, although the absolute magnitude of the shearing rate threshold is over-predicted by the model. Through a normalized predicted scaling, the model demonstrates the dynamic transition into and out of QH-mode qualitatively, within a single plasma discharge. The experimental comparison lends insight into improving the theoretical model by including more accurate geometry and toroidal mode number physics for more accurate quantitative predictions.

I. Introduction

Economical and physically reliable fusion reactor designs require plasma operating regimes that can expel impurities via particle transport, while maintaining high thermal confinement. High confinement (H-mode) plasmas [1] in current machines can maintain these characteristics, with the particle transport enhanced by edge localized modes (ELMs) [2], which are explosive quasi-periodic edge relaxation events thought to develop from magnetohydrodynamic (MHD) instabilities in the edge pedestal region of tokamak plasmas [3]. While H-mode exhibits energy confinement typically a factor of two better than that in low confinement (L-modes) plasmas, ELMs can be detrimental to plasma facing components, and represent a significant challenge for the design and operation of future fusion reactors [4]. As a result, interest has grown significantly in high confinement regimes with intrinsic ELM suppression [5].

There has been considerable progress on developing an alternative to the ELMy H-mode regime, called the quiescent H-mode (QH-mode) [6-9]. In QH-mode, edge fluctuations maintain a quasi-steady edge plasma without explosive relaxation events. QH-mode can operate over broad operational regimes at reactor relevant values of ITER confinement enhancement factors [10] ($H_{98} > 1$), pedestal beta ($\beta_t^{ped} \sim 1\%$), and collisionality ($\nu^* < 0.1$). While further development for QH-mode operation at low torque and rotation is still required, it is considered to be a promising candidate for a naturally ELM free stationary target plasma for fusion power generation [11-12].

The QH-mode edge pedestal is regulated by MHD and/or turbulence that usually spans the width of the pedestal, and is manifested as either 1) a coherent edge harmonic oscillation (EHO), which is a low-n dominated MHD mode usually accessed under high torque conditions, or 2) broadband MHD or electromagnetic turbulence, which can be accessed with lower torque and is often seen in conjunction with a high and wide pedestal [13]. QH-mode operation is typically observed either on or just below the kink-peeling boundary of the peeling-ballooning (PB) stability diagram, as shown for DIII-D discharge #163466 in Fig. (1), which has a coherent EHO.

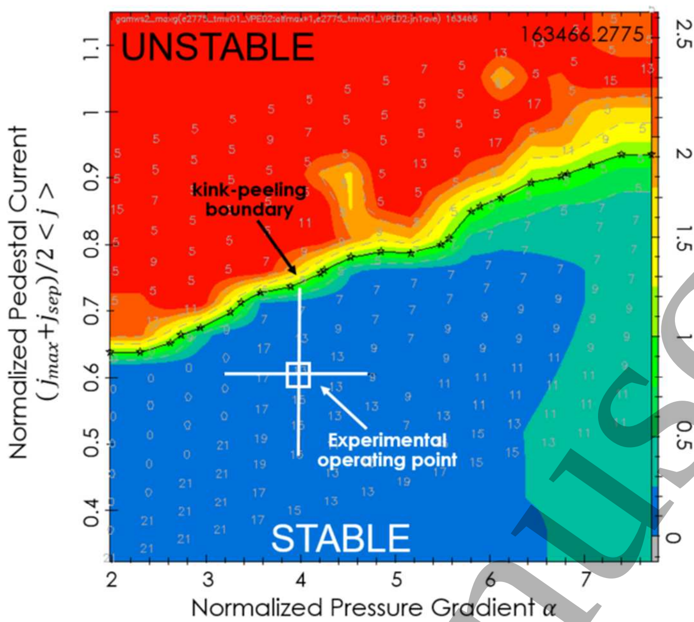

Figure 1: Contour plot of the ratio of the growth rate of the dominant mode calculated by ELITE to half of the ion diamagnetic frequency, ω$_*$, where the horizontal axis is the normalized peak pressure gradient and the vertical axis is the ratio of the average pedestal current to volume averaged current density [14-15]. This peeling-ballooning stability diagram shows the operating point of the DIII-D QH-mode plasma #163466 with a coherent EHO just below the kink-peeling boundary, but stable to ELMs.

Edge pedestal ExB shear is thought to be the principle mechanism for preventing the onset of ELMs and fostering conditions for the more benign QH-mode. When comparing different types of rotation shear, previous studies [16] have shown that there is a threshold for pedestal ExB shear but not for the total carbon rotational shear when describing access to QH-mode versus ELMy H-mode plasmas. Previous research has proposed that the EHO is destabilized by ExB shear and is nonlinearly saturated at the kink-peeling boundary [17-18]. However, the saturation mechanism is not fully understood. Additionally, a nonlinear theory [19] to describe EHO onset has been developed, which models the cross phase dynamics between the radial velocity fluctuations and the PB pressure perturbation, allowing the ExB shear to modulate the edge MHD modes. This paper will analyze and interpret this theory in the context of experimental QH-mode access requirements in Section II; Section III describes DIII-D QH-mode experiments that provide a dataset for testing this theory; Section IV demonstrates that the transition into and out of QH-mode is described qualitatively by the Guo-Diamond theory through profile analysis, showing the theory predicts the existence of an ExB shear threshold for EHO onset. The theoretically predicted scaling of this threshold is consistent with experiment, though the magnitude of the threshold predicted by theory exceeds the experiment result by about a factor of 10^2. Section V discusses possibilities of extending the model for further experimental comparison through magnetic analysis of the EHO measured from the Mirnov coils as well as dynamic heat flux analysis; Section VI summarizes the experiment to theory comparison.

II. Phase evolution model predicting critical ExB shear requirements for QH-mode access

A theory describing the conditions necessary for a QH-mode was derived from synchronization physics [19], where there are many examples in nature, such as fireflies flashing simultaneously; in social behavior like synchronized clapping in a large applauding audience; and in science such as brain rhythms and multi-mode lasers. In the plasma edge pedestal, the synchronization is due to evolution of the phase between pressure and velocity perturbations, $\tilde{p}$ and $\tilde{v_r}$ respectively. The model describes the synchronization and desynchronization elements of the nonlinearly evolved MHD fluctuations in the edge pedestal as due to the evolution of the cross phase in the PB driven heat flux, which is dependent upon the ExB shear.

When the ExB shear is small, the phases are in sync, or in a phase locked state. However, when the ExB shear reaches a critical threshold or higher, it causes the phases to become out of sync and enter a phase slip state. The model predicts a competition between phase pinning and phase winding, where the phase angle regulates the flux and thus the PB induced pedestal relaxation. Phase pinning is the natural tendency for the cross phase to be attracted to a fixed value, which maximizes the flux $< \tilde{v_r}\tilde{p} >$, and corresponds to the cross phase set by MHD. Phase winding is due to the tendency of ExB shear to tilt eddies and increase the phase angle and dominates when the plasma is in the phase slip state ($\frac{dk_r}{dt} = -\partial(k_\perp v_E)/\partial r$, and since $\underline{k} = \underline{\nabla}\Theta$, the phase can be expressed as $\frac{d\Theta}{dt} = k_\perp V_E = k_\perp V_E' \Delta x$). This competition is captured in Eq. (1) [19], which is a variant of the Adler equation [20] and also the mean field equation of the Kuramoto model [21], both of which describe synchronization phenomena.

$$\frac{d}{dt}\Theta_k = k_y V_{ExB}' \Delta x - \frac{|\delta V_{PB,k_x}|}{|\delta P_k|} \langle P \rangle' sin\Theta_k + \tilde{s}_k^\Theta \quad (1)$$

Here Θ_k is the cross phase, k_y is the poloidal wave number, V'_{ExB} is the ExB flow shear driven by the radial electrostatic field, $\delta V_{PB,k_x}$ is the velocity perturbation of the PB modes, and δP_k is the PB pressure perturbation. The mean pressure is denoted by $\langle P \rangle$, and $\tilde{s}_k^{\Theta}$ reflects random phase scatter due to ambient turbulence. The first term on the right hand side represents the winding effect due to shearing, and the second term is the nonlinear pinning term which attracts the phase to its MHD value. Solving Eq. (1) leads to a critical ExB shear V'_{ExB} which is required to "de-pin" the phase, and allow (phase) winding to occur. In this way, the perturbations will become "de-synced". Most transport models address a state of broadband turbulence with a correspondingly short auto-correlation time, for which only slow phase evolution is relevant. However, for a coherent, nonlinearly evolved mode, self-interactions and external influences can combine to induce nontrivial phase evolution, which is addressed in detail in reference 19.

There are three extremal states that this theory predicts for PB modes, which have all been observed experimentally in the DIII-D tokamak, as shown in Fig. (2) in the left column with a schematic of the driven heat flux for each scenario shown in the right column.

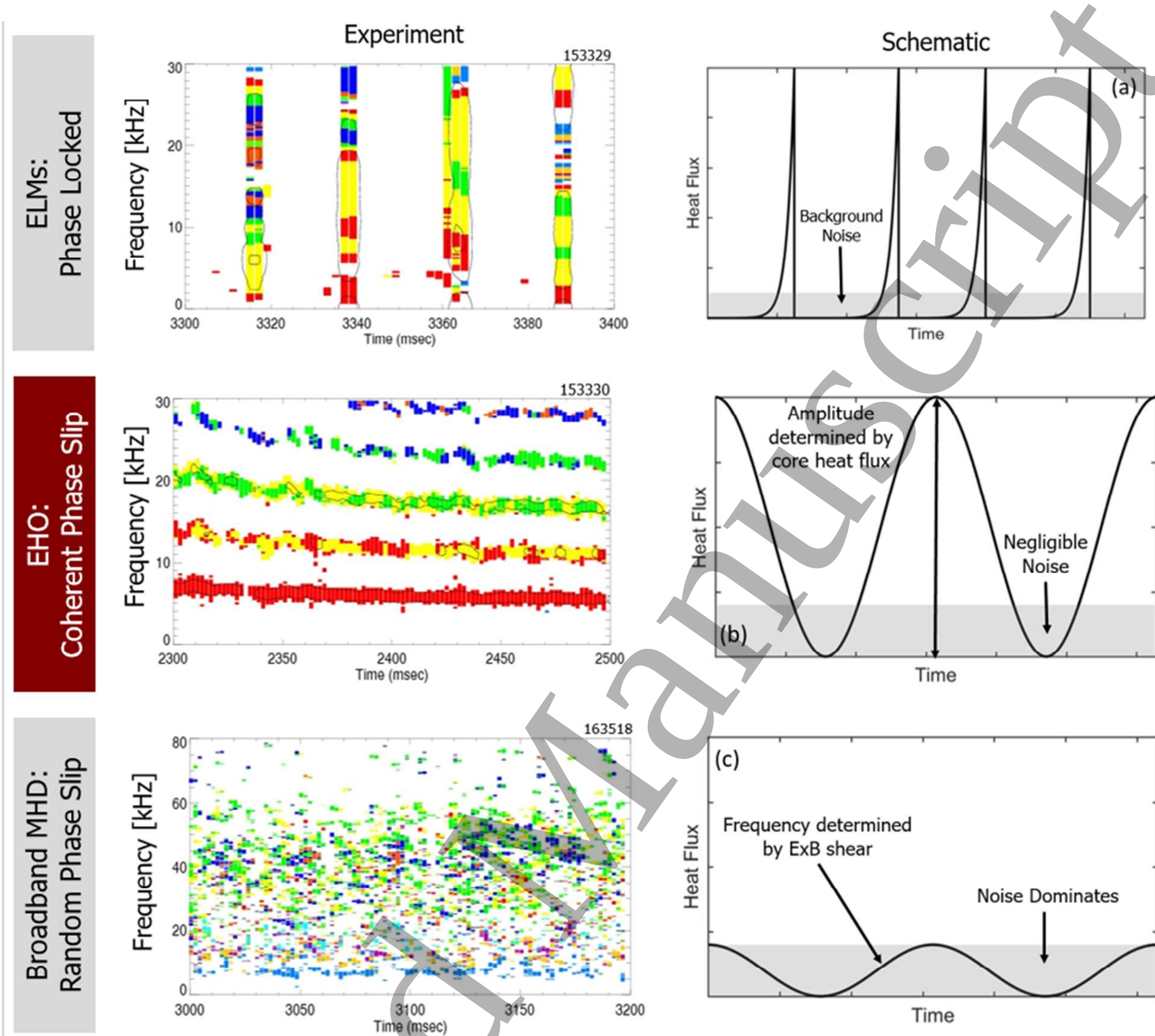

Figure 2: Example magnetic spectra from DIII-D discharges (left column) and the a schematic of the associated heat flux (right column) illustrating the three pedestal states predicted by the Guo-Diamond theory, which are a) phase locked (in sync) perturbations resulting in ELMs b) phase slip (de-synched) perturbations resulting in a coherent EHO c) phase slip with random phase scattering resulting in broadband MHD. The colors denote different toroidal mode numbers. The shaded region in the schematics denotes the noise introduced from phase scatter due to ambient turbulence.

The first state shown in Fig. (2a) occurs when the velocity and pressure perturbations are in sync, or phase locked. This occurs where the second term in Eq. (1) dominates and the cross phase is pinned to its fixed MHD value. In this scenario, the pressure perturbation grows to significant size before strongly modifying ∇p, and corresponds to an ELMy H-mode pedestal.

The heat expulsion is sufficiently violent that the pedestal collapses, and rebuilds again via heating from the core before repeating the cycle. The phase scatter due to ambient turbulence is negligible in this scenario.

The second state predicted by Eq. (1) in Fig. (2b) is when the ExB shear is sufficiently large that the velocity and pressure fluctuations become out of sync and evolve dynamically. In this phase slip state, the pressure perturbation and the flow shear are out of phase, except for short, periodic intervals where $\tilde{v}$ and $\tilde{p}$ are in phase and the PB modes drive heat flux across the pedestal. Experimentally, these short intervals of PB mode pumping strongly resemble the EHO, which emerges naturally from the model through nonlinear phase dynamics that include ExB shear. The frequency of phase slip increases with ExB flow shear and therefore the frequency of the EHO increases with ExB shear (which can experimentally be controlled with externally injected torque), which is in agreement with experimental observations as discussed in Section III. Therefore the frequency of the EHO is modulated by the ExB shear, and the amplitude depends on the PB source from the core and its interaction with the pedestal profile structure. Due to a more steady expulsion of heat (as compared to ELMs), it is possible to sustain a stationary pedestal with an EHO. At strong values of shear, fluctuation amplitudes are suppressed and the phase scatter term is negligible, allowing a robust and coherent EHO to emerge.

The third pedestal state predicted by this theory is one with strong noise, or phase scatter, which stochasticizes the cross phase. This corresponds to a state of broadband MHD and/or electromagnetic turbulence. The broadband MHD case is usually observed at lower ExB shear than the coherent EHO [22], which allows the first and second terms on the right hand side of Eq. (1) to approximately balance. Therefore the cross phase evolution is dominated by the noise term, due to ambient turbulence. Once in this turbulent state, it is predicted that increased ExB shear will drive the edge more towards an EHO state as the winding term begins to dominate. It is possible to have spectrum of states predicted from the model for instances with co-dominant terms in Eq. (1). An example of this would be a coherent EHO observed simultaneously with broadband MHD, which would be an intermediate state to those shown in Fig. (2b) and (2c) through a higher noise level as compared to the amplitude of the PB fluctuation.

At large shear, the model can be further simplified by neglecting the noise term in Eq. (1), yielding a solution for the critical value of ExB shear required for access to a phase slip state, i.e. a critical value of ExB shear for EHO onset [19].

$$\left|V'_{ExB,cr}\right| \approx \tau_A^{-1}\left(1-\epsilon^{\frac{1}{2}}\right)^{\frac{1}{2}} \frac{\beta^{\frac{1}{2}}}{\left|k_y \Delta x\right|}\left(\frac{L_p}{\Delta x}\right)^{\frac{1}{2}} \tag{2}$$

Here $V'_{ExB,cr}$ is the critical ExB rotational shear for the transition between a phase locked and phase slip state, corresponding to an ELMing→QH transition. L_p is the pressure gradient scale length, $\tau_A = L_p/V_A$ is the Alfven time defined with the Alfven velocity, $V_A = B/\sqrt{\mu_0 m_i n_i}$, $\epsilon = a/R$ is the inverse aspect ratio, and $\beta = 2\mu_0\langle P\rangle/B^2$, where B is the total magnetic field, k_y is the poloidal wave number, and Δx is the radial width of the PB mode. The edge pedestal region is assumed to be near marginally stable to peeling-ballooning modes with a pressure perturbation driven by the heat flux from the core, and the ExB flow shear is assumed to be the mean flow shear in the pedestal region.

III. DIII-D experiments for critical ExB shear

In order to study the relationship between ExB shear and the existence of the EHO, a series of DIII-D discharges were developed in upper single null divertor configuration, with low density and high power injection to access the low collisionality kink-peeling boundary. The external torque was varied at constant heating power by varying the mix of neutral beam injection (NBI) with and against the plasma current (co-Ip vs. counter-Ip). Waveforms for a typical discharge are shown in Fig. (3). Large counter-Ip torque is injected in the early phase of discharge formation particularly before the L-H transition time to establish the EHO for robust QH-mode operation. The NBI counter-Ip torque is ramped down at constant $\beta_N = \beta/(I_p/aB)$ to investigate the EHO ExB shear threshold. When the ExB shear becomes sufficiently small, the coherent EHO disappears and ELMs appear. The counter-Ip torque is then increased again until the QH-mode is reestablished. The time traces for injected torque, the maximum Hahm-Burrell ExB shearing rate in the outer shear layer of the radial electric field in the edge pedestal region [1,23], EHO amplitude for n=1 and n=2 toroidal mode numbers (usually dominant), and the EHO spectrogram signals are shown in Fig. (3a-d) for DIII-D discharge #163466.

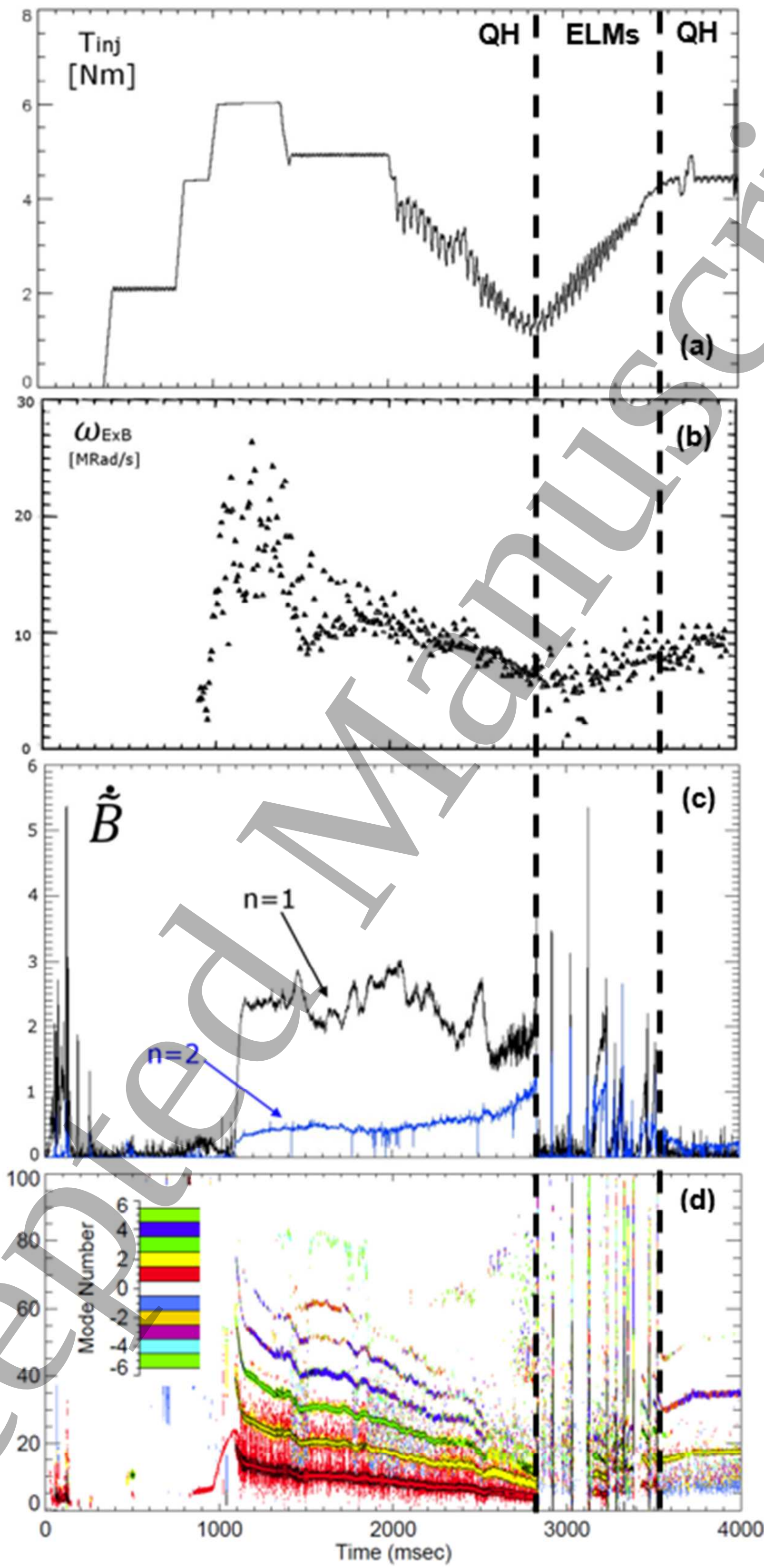

Tinj [Nm]
QH
ELMs
QH
(a)
ω_{ExB} [MRad/s]
(b)
$\dot{\tilde{B}}$
(c)
n=1
n=2
(d)
Mode Number
Time (msec)

Figure 3: Time series traces from DIII-D shot #163466 for a) external counter torque injection b) maximum Hahm-Burrell shearing rate in the outer shear layer of the Er well in the edge pedestal c) RMS amplitude of magnetic signal from the Mirnov coils for n=1 and n=2 dominant modes d) magnetic spectrogram from the Mirnov coils.

As the torque decreases (Fig. 3a), the ExB shear in the edge pedestal region also decreases (Fig. 3b) until the onset of ELMs. The EHO can be seen through the magnetic measurements (Fig. 3c) as an n=1 dominant mode before ELM onset, but returns as n=2 dominant after QH-mode is reestablished with increased torque. The magnetic signatures show the coherent oscillations of many harmonics of the EHO (Fig. 3d) decreasing in frequency as the torque is ramped down toward the ELM state, as is consistent with the model described in Section II.

Two sets of torque ramping experiments were performed with toroidal magnetic fields and plasma currents of 2T/1MA and 1.4T/0.73MA at constant safety factor at the 95% flux surface, q_{95}~5, to determine scaling trends for the critical ExB shear required to sustain a QH-mode. For pedestal analysis, data was averaged over 50ms directly before the ELMs begin, and also after they cease and QH-mode is re-established, in order to calculate the critical ExB shear for both QH→ELMing and ELMing→QH transitions. Example pedestal profiles for the two different toroidal magnetic fields are shown in Fig. (4).

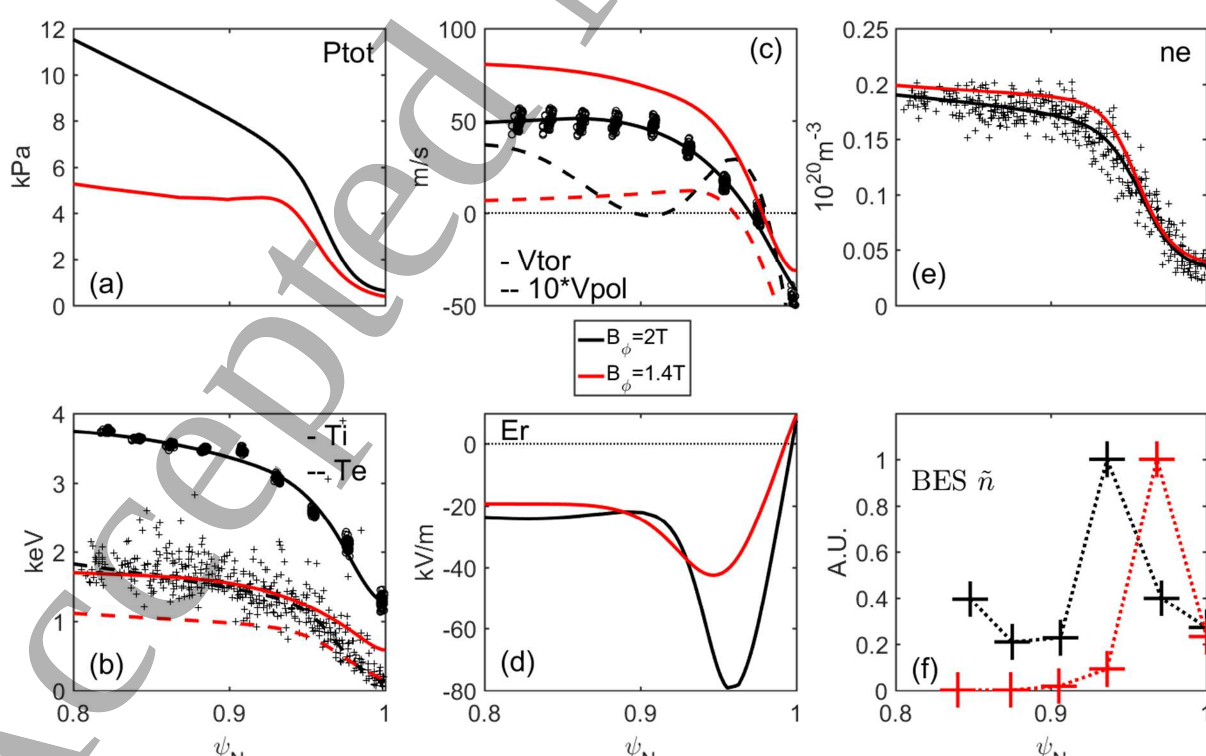

Figure 4: Edge pedestal profiles at the QH→ELM transition for $B_\phi = 2T$ (black) and $B_\phi = 1.4T$ (red) as a function of normalized poloidal flux ψ_N for DIII-D shots #163466/91, respectively. Panels show a) total pressure b) ion and electron temperature c) toroidal and poloidal carbon velocity d) radial electric field e) electron density and f) normalized EHO density fluctuation from beam emission spectroscopy.

The two different magnetic field discharges have similar density pedestals, but the 2T case has a significantly larger ion temperature pedestal, leading to a larger pressure pedestal and radial therefore electric field well. Both discharges have ratios of $T_i/T_e > 1.5$, showing the relatively low coupling between ions and electrons. The 1.4T discharge has a larger toroidal velocity, but significantly less shear in the poloidal velocity profile. The EHO density fluctuations measured through beam emission spectroscopy show the fluctuations localized to the pedestal region.

To compare experimental measurements to the Guo-Diamond theory in Section II, 26 torque ramping discharges similar to shots #163466/91 were analyzed to yield 43 critical ExB shear data points describing a QH→ELMing or ELMing→QH transition.

IV. Comparison of experimental ExB critical shear requirements to plasma parameters predicted by theory – Profile Analysis

The ExB frequency shown in Fig. (3b) is defined by the Hahm-Burrell shearing rate [24], $\omega_{ExB} = \frac{(RB_p)^2}{B}\partial\left(\frac{E_r}{RB_p}\right)/\partial\psi$. This is the quantity usually used for edge pedestal analysis due to its rigorous treatment of flux expansion in the edge region, but is not a direct comparison to the theory described in Section II. The Guo-Diamond theory is based on a simple cylindrical geometry model as well as the assumption of an average flow shear over the shear layer instead of the local maximum value for the inner shear layer, which has been typical in previous analysis [25]. The edge ExB shear calculated from experiment that is a direct comparison to theory is shown in Eq. (3) through the spatial derivative of the radial momentum balance equation normalized by the total magnetic field.

$$V'_{ExB} = \left(\frac{Er}{B}\right)' = -\frac{V'_\phi B_\theta}{B} + \frac{V'_\theta B_\phi}{B} + \left(\frac{\langle P\rangle'}{enB}\right)' \qquad (3)$$

For V'_{ExB} in Eq. (3) to be evaluated as a constant field over the edge pedestal region, the average derivative of the quantity E_r/B is taken in the entire edge region is defined by $\Delta(\mathrm{E_r}/B)/\Delta r$ calculated from a modified double tanh fit (two combined mtanh fits described in Fig. 1 of reference 26 for both the inside and outside of the Er well in Fig. 5) of CER data using the outer side of the radial electric field well, shown in Fig. (5) for the 2T DIII-D discharge #163471. The outer shear layer, shown by the shaded region in Fig. (5), was chosen due to the correlation of the outer radial electric field shear with QH-mode access demonstrated from previous research [16]. The average inner shear layer showed little trend with the predicted model parameters, and therefore the outer shear layer is presented due to the more interesting observed correlation. It should be noted that for wide pedestal QH-mode experiments with broadband MHD, it is observed that the local ExB shear on the inside of the Er well plays a role [22] in determining the turbulent state, indicating further research is needed to understand the local versus global pedestal ExB shear requirements in QH-mode.

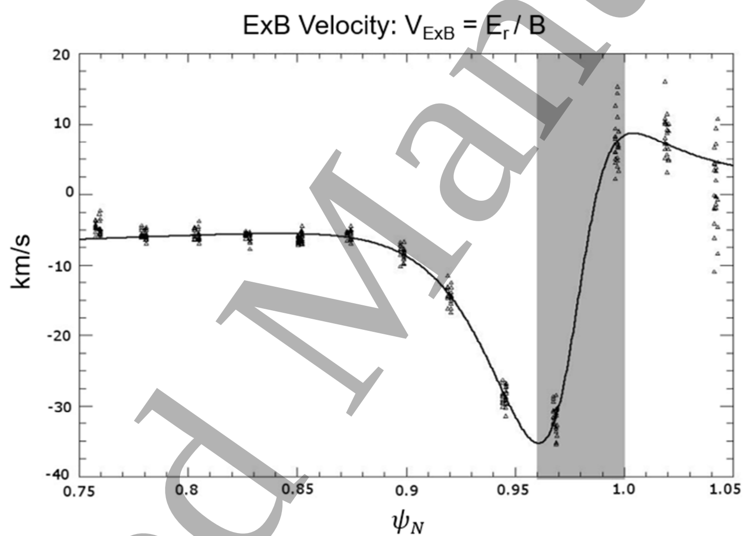

Figure 5: Er/B profile at the QH → ELM transition from DIII-D shot #163471 showing the outer shaded region where the ExB shear is calculated for the 2T discharge.

The expression for critical shear in Eq. (2) can be simplified to Eq. (4) by using the definitions $\beta = 2(n_i T_i + n_e T_e)/B^2$ and $c_s = \sqrt{\frac{2(T_i+T_e)}{m_i}}$ and assuming 1) $n_e = n_i$, which are less than 10% different for the current shot comparisons, and 2) $k_y \Delta x \cong 0.1$. The width of the mode is taken from BES measurements from Fig. (4f), but it should be noted that this should be derived from the displacement profile instead of density fluctuation profiles for more accurate analysis.

$$|V'_{ExB}| = \frac{\left(1-\epsilon^{\frac{1}{2}}\right)^{\frac{1}{2}}}{|k_y\Delta x|}\left[\frac{2(T_i+T_e)}{m_i L_p \Delta x}\right]^{1/2} \tag{4}$$

A simplified normalized scaling with respect to the changing experimental parameters and proportional to the constant α can then be expressed.

$$|V'_{ExB}| = \alpha \frac{c_s}{\sqrt{L_p \Delta x}} \tag{5}$$

Eq. (5) is evaluated with the ion acoustic velocity at the top of the pedestal, and the average pressure gradient scale length between the pedestal top and the separatrix, $\overline{L_p} = \int_{ped}^{sep} L_p dr / \int_{ped}^{sep} dr$. Average pedestal gradients were chosen for consistency with the model assuming perturbations occur within a static background field, while the pedestal temperature was chosen at the pedestal top as a representative quantity defining the QH-mode pedestal, and is reasonably within a factor of two of other characteristic temperatures. The comparison of the experimental shear to the theoretical scaling Eq. (5) for all 43 data points is shown in Fig. (6), where the proportionality constant is $\alpha = 0.14$ when fit to the data, and is a normalization factor to the model, and not the slope of the trend line shown in Fig. (6). Therefore, the order of magnitude over-estimation of the predicted critical shearing rate as compared to the experimental critical shearing rate is seen to be about two orders of magnitude via $\alpha k_y \Delta x / \sqrt{1-\epsilon^{\frac{1}{2}}} \sim 0.012$.

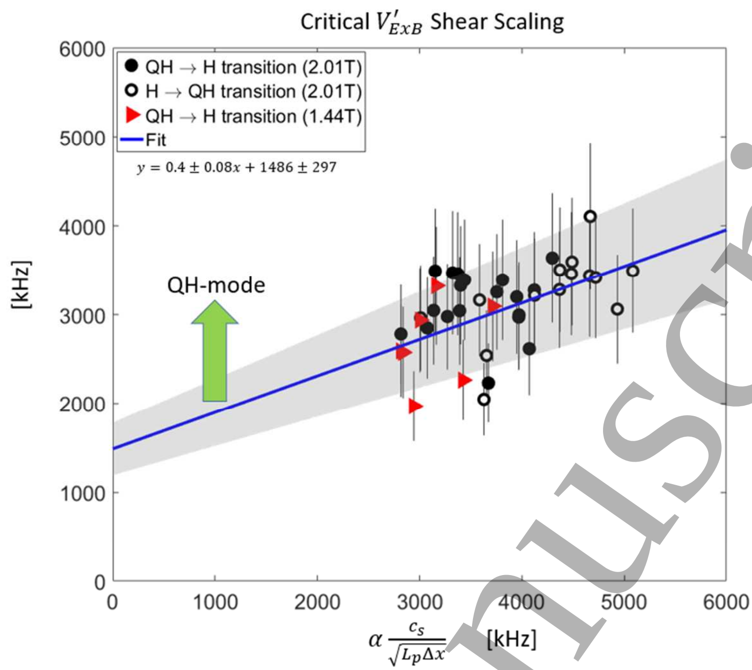

Figure 6: Normalized scaling of experimental ExB rotational shear with parameters predicted by the Guo-Diamond nonlinear phase slip theory.

The closed black circles in Fig. (6) represent the QH→ELMing transition for 2T magnetic field discharges, and the closed red triangles represent the QH→ELMing transition for the 1.4T discharges. The open black circles represent the ELMing→QH transition for the 2T shots. Even though a hysteresis in total externally injected NBI torque was observed in experiment, the equality of the ELMing-EHO and EHO-ELMing transition thresholds in the phase space defined by the critical ExB shear and the Guo-Diamond scaling parameter is suggestive of the absence of hysteresis in that transition. Hysteresis is indicative of a "memory" in the dynamics. For example, the familiar hysteresis in L-H and H-L transitions is likely related to the difference between the transport processes in L and H mode, so that a "memory" of the H-mode state leads to its persistence. In the case of the ELMing-EHO (and reverse) transition, an interpretation could be that the apparent absence of memory may be indicative of an ideal MHD process (such as kinking and unkinking) in the underlying peeling mode evolution. However, much further work is required to investigate and substantiate this speculation.

The critical ExB shear calculated from the theoretical scaling of Eq. (5) with α taken from the experimental fit acts as a threshold for QH-mode access. The fit to these data points notably has a y-intercept, which may be caused by a local Doppler shift at the reference mode surface neglected by the Guo-Diamond model. Robust QH-mode plasmas will lie in the parameter space well above these critical values. Taking shot #163466 as an example and adding data points throughout the discharge, the evolution of the QH-mode can be tracked in the phase space defined by ExB shear and the normalized Guo-Diamond scaling. Time slices numbered #1-3 shown in Fig. (7a) are early in the discharge in QH-mode (pink) and are shown to lie above the critical shear line in Fig. (7b) because of the high ExB shear generated from significant external torque. As torque is ramped downwards, the shear approaches the critical value at time slice #4, and denotes the change in edge turbulence from a phase slip to a phase locked state. As the torque ramps back up, time slice #5 shows the transition back into QH-mode with increased shear. Time slice #6 shows a later point in the discharge with increased ExB shear. The operating point returns to a similar location as the beginning of the discharge.

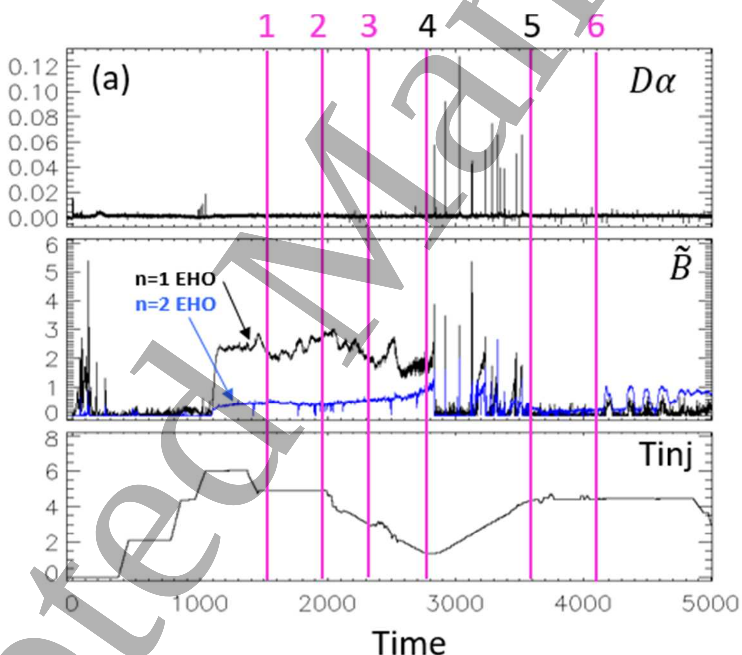

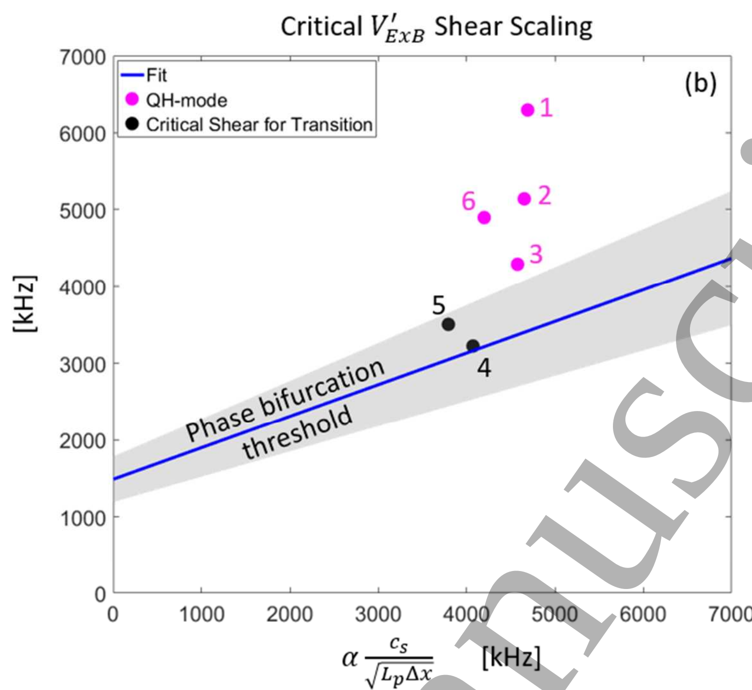

Figure 7: a) Time history of DIII-D discharge #163466 showing the D-alpha trace illustrating the onset of ELMs, the n=1 and n=2 magnetic fluctuations from the Mirnov coils, and injected torque. b) Evolution of the same shot in the phase space defined by ExB shear and the Guo-Diamond scaling parameters. The discharge starts in a robust QH-mode and ramps towards the threshold defined by the critical shear scaling as torque is decreased.

The transition into and out of QH-mode in Fig. (7) is described qualitatively by the Guo-Diamond theory. This demonstrates the theory can predict the existence of an ExB shear threshold, that when normalized, is consistent with experiment. When calculating the absolute critical ExB velocity from Eq. (4), the predicted values overestimate the experimental values by a factor of ~10^2 as expressed through the constant normalization parameter α applied uniformly across the entire dataset. The phase space defined by the Guo-Diamond scaling parameter and the critical ExB shearing rate maps out a region where QH-mode can exist and where there is not enough shear sufficient to maintain an EHO. The pink data points denoting a non-marginal QH-mode are separated sufficiently far away and outside of the error of the fit curve from the where the critical data points in black lie in the phase space given similar plasma conditions in the same discharge. This emphasizes that there is no intrinsic dependence of the calculated critical ExB shear and the theoretically predicted plasma parameters (e.g. through momentum balance requirements). Figure 7 emphasizes that the Guo-Diamond model is able to define a phase space, though normalized, where QH-modes can reside and where they cannot (below the line), which is an important advancement from previous research.

The critical ExB shear scales with related quantities to the Guo-Diamond theory such as pedestal temperature and collisionality shown in Fig. (8), though does not appear to be correlated with other quantities like the pedestal density and pressure gradient scale length alone. The dashed lines are power law least squares fits of the form $y = e^a x^b$.

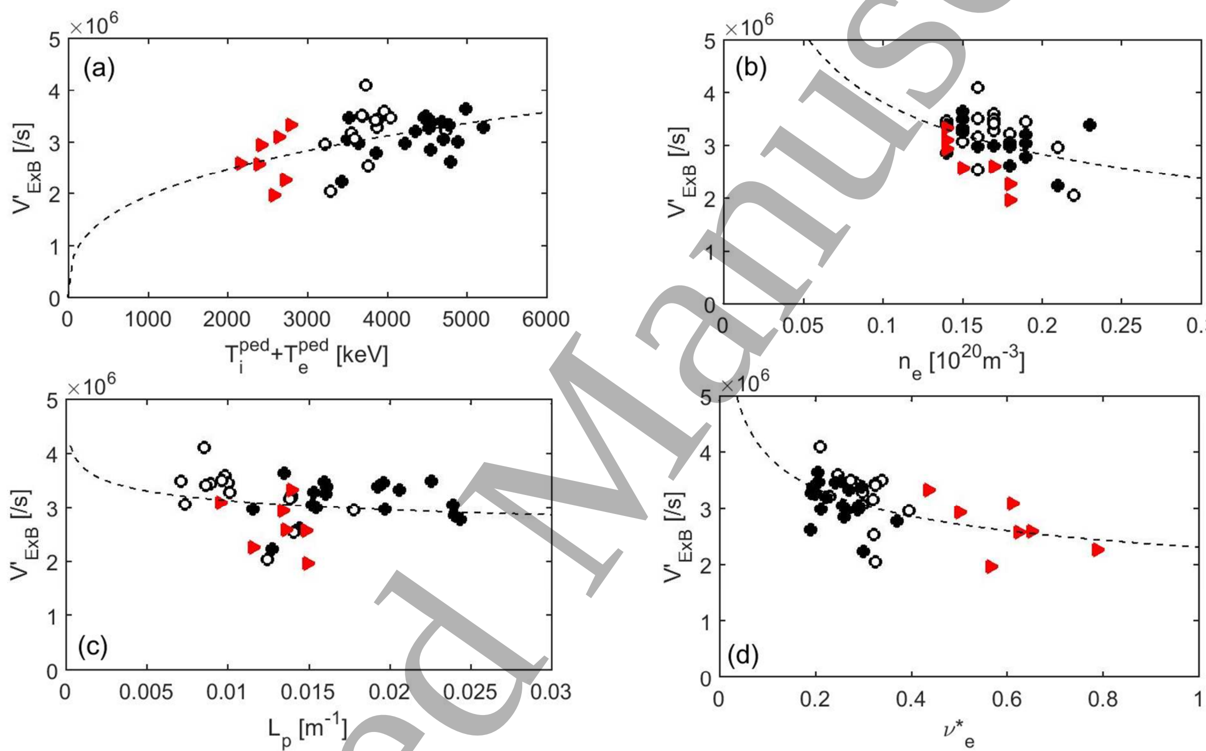

Figure 8: Experimental critical ExB shear scaling with a) Ti+Te b) pedestal density c) pedestal pressure gradient scale length and d) pedestal collisionality

In Fig. (8a), the QH→ELMing transitions at 2T are shown to have preferentially higher temperature than after the back transition ELMing→QH when the plasma has experienced a period of ELMs. The 1.4T discharges are seen to have systematically lower temperature than the 2T plasmas, which is consistent with the pedestal analysis shown in Fig. (4). There is no notable scaling trend with pedestal density or pressure gradient scale length, though the data is ordered similarly to the Guo-Diamond scaling with total pedestal temperature and pedestal collisionality, which are parameters that appear or are related to those predicted in the theoretical scaling. There is a slightly negative trend for the critical shearing rate as collisionality increases, which should be noted is opposite to that observed by similar analysis for the local Hahm-Burrell shearing rate evaluated at the inner shear layer of the radial electric field [25].

V. Suggested improvements, extensions, and interpretations of the Guo-Diamond model

The purpose of this article is to present a detailed comparison of experimental QH-mode data from DIII-D with the proposed Guo-Diamond theoretical model. This section covers possible improvements to the model, though not the rigorous implementation through re-assessing the theory, which would be necessary for a quantitative estimate of these proposed improvements, but is outside the scope of this comparison. The Guo-Diamond model predicts the threshold scaling trends for the QH→ELMing transition, though improvements to the theory are required in order to predict the absolute magnitude of the critical ExB shear threshold. Several assumptions in both the model and experimental comparison that could lead to the over-estimation of the absolute value of the critical shear (but not necessarily explicitly account for the over-estimation of the experimental shearing rate values) are proposed: 1) geometry 2) interpretation of poloidal wave number 3) calculation of PB mode width 4) higher order nonlinear terms 5) measurement and fitting uncertainty. The Guo-Diamond model assumes cylindrical geometry in a region of the plasma where toroidal geometric effects can significantly influence local parameters [24]. The assumption of a constant ExB shear field in the background plasma also simplifies the ExB profile structure observed experimentally in the edge. Additionally, there is no explicit toroidal mode number scaling present in the calculation for the ExB shear, yet it implicitly appears through quantities like the PB mode width and poloidal wave number, k_y which can nominally be estimated as $k_y \sim nq/r$. Various dominant EHO harmonics are seen under different plasma conditions in experiment and have different critical ExB shear requirements, so expanding understanding of the toroidal mode number physics and its inclusion in the theory is important for future model improvements. Another assumption in the model evaluation was that the radial width of the mode was calculated through the density fluctuation measured from beam emission spectroscopy, though the theory is derived using the plasma displacement as the key parameter defining the PB mode structure. It is also possible there are hidden geometrical factors within the mode width calculation, such as a modified radial mode width as a function of plasma toroidal mode number, triangularity, elongation, or q_{95}, which would need to be explored through modeling and experiments. Furthermore, higher order terms may also be included to improve the model such as the nonlinear response of the pressure perturbation to the ExB shear perturbation; more rigorous analysis is required to determine their relevance and potential impact. Lastly, there is experimental uncertainty in the profile measurements and fitting of the ExB shear, as seen in Fig. (5) where there are limited CER measurements in the edge pedestal region. Previous experiments [25] have used outer gap sweeps for high CER resolution, which may be beneficial for similar analysis in the future. The focus of this experimental comparison of the Guo-Diamond model has been through the edge pedestal ExB shear, which has led to insights on possible extensions or interpretations of the model for future experimental evaluations. With further development, the Guo-Diamond model could be used to predict other measurable quantities such as the EHO frequency measured from external magnetic coils and pedestal heat flux dynamics.

The frequency of the EHO measured by magnetics could be a possible alternative experimental analysis to profile fitting of the experimental ExB shear because the EHO frequency can be predicted by the Guo-Diamond theory.

$$\Omega_{slip} = \Omega_{EHO} \approx k_y \Delta x\, V'_{ExB} \tag{6}$$

If this phase slip frequency is defined at the critical ExB shear value, then Eq. (2) can be substituted for the shearing rate to obtain an absolute scaling for the EHO critical frequency observed in the lab frame of reference.

$$f_{EHO,cr} = \frac{\Omega_{EHO,cr}}{2\pi} \approx \frac{k_y \Delta x V'_{ExB,cr}}{2\pi} = \sqrt{\frac{\left(1-\epsilon^{\frac{1}{2}}\right)(T_i+T_e)}{2\pi^2 m_i L_p \Delta x}} \tag{7}$$

This may have a more complicated interpretation when comparing to magnetic signals from Mirnov coils because many processes beyond phase slip can impact the measured frequency (e.g. Doppler shift from toroidal and poloidal rotation, location of coils, etc.). The Guo-Diamond model predicts a phase slip frequency of zero at the critical transition between QH-mode and ELMs, though experimentally an EHO of a few kilohertz is observed. Evaluating the absolute scaling from Eq. (7) yields frequencies which are a factor of $\sim 10^3$ larger than those measured experimentally around 1-20 kHz, which is consistent with the order of magnitude over-estimation using the profile analysis methodology in Section IV. This highlights the motivation for improving the model to allow for direct comparison to magnetic signals from Mirnov coils, which would provide a tool for understanding QH-mode access requirements with limits on the relationship between externally injected torque and experimental EHO frequency that would have potential to be extrapolated for real-time analysis.

The profile analysis showing the transition into and out of QH-mode in Section IV and the formulation of the Guo-Diamond model as a phase evolution equation hints at the capability of extending the theory to predict dynamic quantities. The EHO frequency can be predicted as mentioned above, which could further be extended to heat flux dynamics to analyze evolution of pedestal transport across both transport and fluctuation time scales.

VI. Conclusion

There is experimental evidence of a critical value of edge ExB shear required for a QH-mode to sustain an edge harmonic oscillation and ELM-free state. Experimental critical shear values from torque ramping experiments on DIII-D are compared to a model for the EHO which describes the evolution of the cross phase between the perturbations of $\tilde{v}_r$ and $\tilde{p}$. This theory predicts three states of edge pedestal turbulence 1) coherent EHO caused by a phase slip modulated by the ExB shear (out of sync fluctuations) 2) ELMs caused by a locked phase state (in sync fluctuations) and 3) broadband MHD turbulence. This is the first theory to predict a critical ExB shear threshold requirement for QH-mode, which agrees with experimental observations. The model can be simplified in order to be quantitatively compared to experiment to predict the ExB shear at the transition between QH→ELMing and ELMing→QH modes to demonstrate a scaling with $\alpha\, c_s/\sqrt{L_p \Delta x}$, where α is a normalization constant, c_s is the ion acoustic velocity, and Δx is the radial width of the peeling-ballooning mode. The DIII-D dataset of critical ExB shearing rates for QH-mode access compared to the Guo-Diamond theory shows that the model a) predicts threshold scalings consistent with experimental data b) over-predicts the absolute magnitude of the ExB shear threshold by two orders of magnitude, and c) indicates the absence of hysteresis in the QH→ELMing and ELMing→QH transition thresholds d) qualitatively demonstrates the transition into and out of QH-mode through the normalized scaling and defines a phase space that describes where QH-mode can exist with respect to the predicted model parameters e) provides a conceptual framework to analyze the mechanisms that allow QH-mode to be naturally ELM-stable.

There are several assumptions in both the model and experimental comparison that could lead to the over-estimation of the absolute value of the critical shear including 1) geometry 2) interpretation of poloidal wave number 3) calculation of PB mode width 4) higher order nonlinear terms, and 5) measurement and fitting uncertainty. Assessing and improving these assumptions is essential for better quantitative agreement of the theoretical prediction for the absolute value of the ExB shear threshold with experimentally measured values. Lastly, experimental comparisons of the edge pedestal ExB shear to the predicted Guo-Diamond model parameters lead to insights on extending the model for dynamic analysis of other quantities such as the EHO frequency measured from external magnetic coils and pedestal heat flux.

Acknowledgements

The efforts of the DIII-D team was essential to this work and greatly appreciated. This research was supported by the U.S. Department of Energy, Office of Science, and Office of Fusion Energy Sciences using the DIII-D National Fusion Facility under award DE-FC02-04ER54698 and MIT cooperative agreement DE-SC0014264.

Disclaimer

References

[1] F. Wagner, G. Becker, K. Behringer, D. Campbell, A. Eberhagen, W. Engelhardt, G. Fussmann, Gehre, J. Gernhardt, G. v. Gierke, G. Haas, M. Huang, F. Karger, M. Keilhacker, Q. Kluber, M. Kornherr, K. Lackner, G. Lisitano, G. G. Lister, H. M. Mayer, D. Meisel, E. R. MIiller, H. Murmann, H. Niedermeyer, W. Poschenrieder, H. Rapp, H. Bohr, F. Schneider, G. Sil.ler, E. Speth, A. Stabler, K. H. Steuer, G. Venus, O. Vollmer, and Z. Yu, PRL **49**, 1408 (1982)

[2] A. Leonard, PoP **21**, 090501 (2014)

[3] P.B. Snyder, H.R. Wilson, J.R. Ferron, L.L. Lao, A.W. Leonard, D. Mossessian, M. Murakami, T.H. Osborne, A.D. Turnbull and X.Q. Xu, Nucl. Fusion **44**, 320 (2004)

[4] A. Loarte, G. Saibene, R. Sartori, D. Campbell, M. Becoulet, L. Horton, T. Eich, A. Herrmann, G. Matthews, N. Asakura, A. Chankin, A. Leonard, G. Porter, G. Federici, G. Janeschitz, M. Shimada, and M. Sugihara, PPCF **45**, 1549 (2003)

[5] R. Maingi, Nucl. Fusion **54**, 114016 (2014)

[6] K.H. Burrell, M.E. Austin, D.P. Brennan, J.C. DeBoo, E.J. Doyle, P. Gohil, C.M. Greenfield, R.J. Groebner, L..L. Lao, T.C. Luce, M.A. Makowski, G.R. McKee, R.A. Moyer, T.H. Osborne, M. Porkolab, T.L. Rhodes, J. Rost, M.J. Schaffer, B.W. Stallard, E.J. Strait, M.R. Wade, G. Wang, J.G. Watkins, W.P. West, and L. Zeng, PPCF **44**, A253 (2002)

[7] K.H. Burrell, M. E. Austin, D. P. Brennan, J. C. DeBoo, E. J. Doyle, C. Fenzi, C. Fuchs, P. Gohil, C. M. Greenfield, R. J. Groebner, L. L. Lao, T. C. Luce, M. A. Makowski, G. R. McKee, R. A. Moyer, C. C. Petty, M. Porkolab, C. L. Rettig, T. L. Rhodes, J. C. Rost, B. W. Stallard, E. J. Strait, E. J. Synakowski, M. R. Wade, J. G. Watkins, and W. P. West, PoP **5**, 2153 (2001)

[8] K.H. Burrell, W. P. West, E. J. Doyle, M. E. Austin, T. A. Casper, P. Gohil, C. M. Greenfield, R. J. Groebner, A. W. Hyatt, R. J. Jayakumar, D. H. Kaplan, L. L. Lao, A. W. Leonard, M. A. Makowski, G. R. McKee, T. H. Osborne, P. B. Snyder, W. M. Solomon, D. M. Thomas, T. L. Rhodes, E. J. Strait, M. R. Wade, G. Wang, and L. Zeng, PoP **12**, 056121 (2005)

[9] K.H. Burrell, A.M. Garofalo, W.M. Solomon, M.E. Fenstermacher, D.M. Orlov, T.H. Osborne, J.-K. Park, and P.B. Snyder, Nucl. Fusion **53**, 073038 (2013)

[10] ITER Physics Basis Expert Groups on Confinement and Transport and Confinement Modelling and Database, ITER Physics Basis Editors 1999 Nucl. Fusion 39 (2175)

[11] A.M. Garofalo, K. H. Burrell, D. Eldon, B. A. Grierson, J. M. Hanson, C. Holland, G. T. A. Huijsmans, F. Liu, A. Loarte, O. Meneghini, T. H. Osborne, C. Paz-Soldan, S. P. Smith, P. B. Snyder, W. M. Solomon, A. D. Turnbull, and L. Zeng, PoP **22**, 056116 (2015)

[12] W.M. Solomon, K.H. Burrell, M.E. Fenstermacher, A.M. Garofalo, B.A. Grierson, A. Loarte, G.R. McKee, R. Nazikian, T.H. Osborne, and P.B. Snyder, Nucl. Fusion **55**, 073031 (2015)

[13] K.H. Burrell, K. Barada, X. Chen, A. M. Garofalo, R. J. Groebner, C. M. Muscatello, T. H. Osborne, C. C. Petty, T. L. Rhodes, P. B. Snyder, W. M. Solomon, Z. Yan, and L. Zeng, PoP **23**, 056103 (2016)

[14] H.R. Wilson, P. B. Snyder, G. T. A. Huysmans, and R. L. Miller, Phys. Plasmas **9**, 1277 (2002)

[15] P.B. Snyder, H. R. Wilson, J. R. Ferron, L. L. Lao, A. W. Leonard, T. H. Osborne, A. D. Turnbull, D. Mossessian, M. Murakami, and X. Q. Xu , Phys. Plasmas **9**, 2037 (2002)

[16] A.M. Garofalo, W.M. Solomon, J.-K. Park, K.H. Burrell, J.C. DeBoo, M.J. Lanctot, G.R. McKee, H. Reimerdes, L. Schmitz, M.J. Schaffer, and P.B. Snyder, Nucl. Fusion **51**, 083018 (2011)

[17] P.B. Snyder, K.H. Burrell, H.R. Wilson, M.S. Chu, M.E. Fenstermacher, A.W. Leonard, R.A. Moyer, T.H. Osborne, M. Umansky, W.P. West, and X.Q. Xu, Nucl. Fusion **47**, 961 (2007)

[18] Xi Chen, K.H. Burrell, N.M. Ferraro, T.H. Osborne, M.E. Austin, A.M. Garofalo, R.J. Groebner, G.J. Kramer, N.C. Luhmann Jr, G.R. McKee, C.M. Muscatello, R. Nazikian, X. Ren, P.B. Snyder, W.M. Solomon, B.J. Tobias, and Z. Yan, Nucl. Fusion **56**, 076011 (2016)

[19] Z.B. Guo and P.H. Diamond, PRL **114**, 145002 (2015)

[20] R. Adler, Proc IRE **34**, 351 (1946)

[21] J.A. Acebron, L. L. Bonilla, Conrad J. Pérez Vicente, Félix Ritort, and Renato Spigler, Rev. Mod. Phys. 77, 137 (2005)

[22] Xi Chen, K.H. Burrell, T.H. Osborne, W.M. Solomon, K. Barada, A.M. Garofalo, R.J. Groebner, N.C. Luhmann, G.R. McKee, C.M. Muscatello, M. Ono, C.C. Petty, M. Porkolab, T.L. Rhodes, J.C. Rost, P.B. Snyder, G.M. Staebler, B.J. Tobias, Z. Yan and the DIII-D Team, Nucl. Fusion **57**, 022007 (2017)

[23] K.H. Burrell, PoP **4**, 1499 (1997)

[24] T.S. Hahm and K.H. Burrell, PoP **2**, 1648 (1995)

[25] Xi Chen, K.H. Burrell, T.H. Osborne, K. Barada, N.M. Ferraro, A.M. Garofalo, R.J. Groebner, G.R. McKee, C.C. Petty, M. Porkolab, T.L. Rhodes, J.C. Rost, P.B. Snyder, W.M. Solomon, Z. Yan, and The DIII-D Team, Nucl. Fusion **57**, 086008 (2017)

[26] R.J. Groebner and T.N. Carlstrom, PPCF 40, 673-677 (1998)